Electronic Supplementary Material (ESI) for Journal of Materials Chemistry A.

Supporting information

Hybrid water vapor sorbent design with pollution shielding property: extract clean water from polluted bulk water sources

Renyuan Li[1], Mengchun Wu[1], Yusuf Shi[1], Sara Aleid[1], Wenbin Wang[1], Chenlin Zhang[1], Peng Wang[1,2,*]

1. Water Desalination and Reuse Center, Division of Biological and Environmental Science and Engineering, King Abdullah University of Science and Technology, Thuwal 23955-6900, Saudi Arabia.

2. Hong Kong Polytechnic University, Hung Hom, Kowloon, Hong Kong, China

* Corresponding author: peng.wang@kaust.edu.sa; peng1.wang@polyu.edu.hk

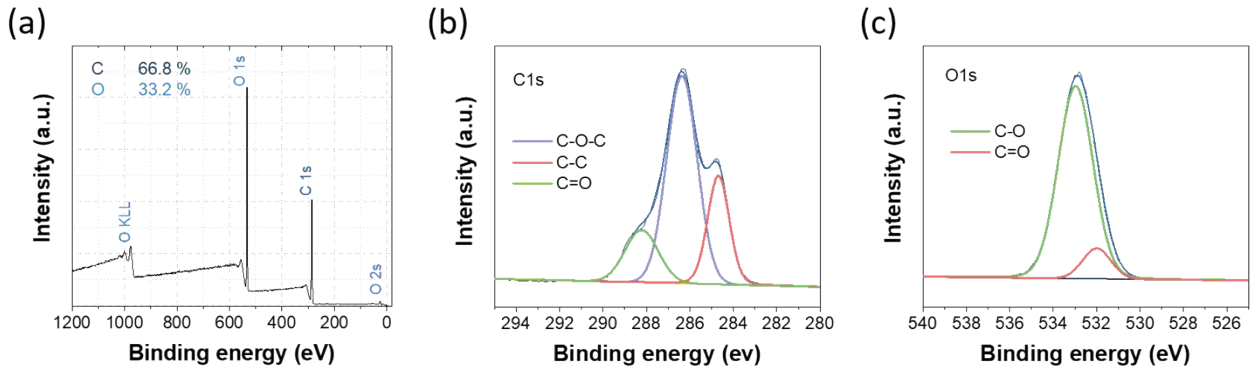

Figure S1. XPS spectra of cotton fabric. (a) Survey spectra. High-resolution spectra of (b) C1s and (c) O1s.

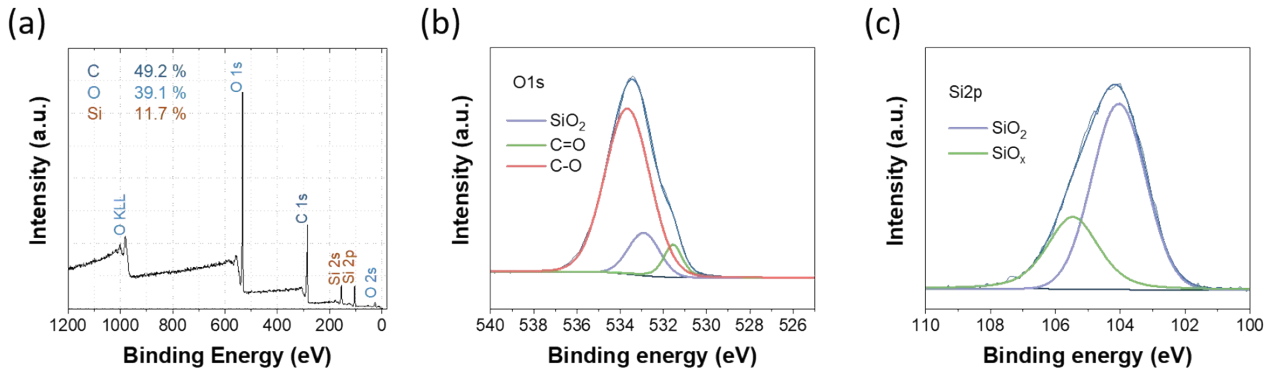

Figure S2. XPS spectra of the elements of SiO_2@cotton. (a) Survey spectra. High-resolution of (b) O1s and (c) Si2p spectra.

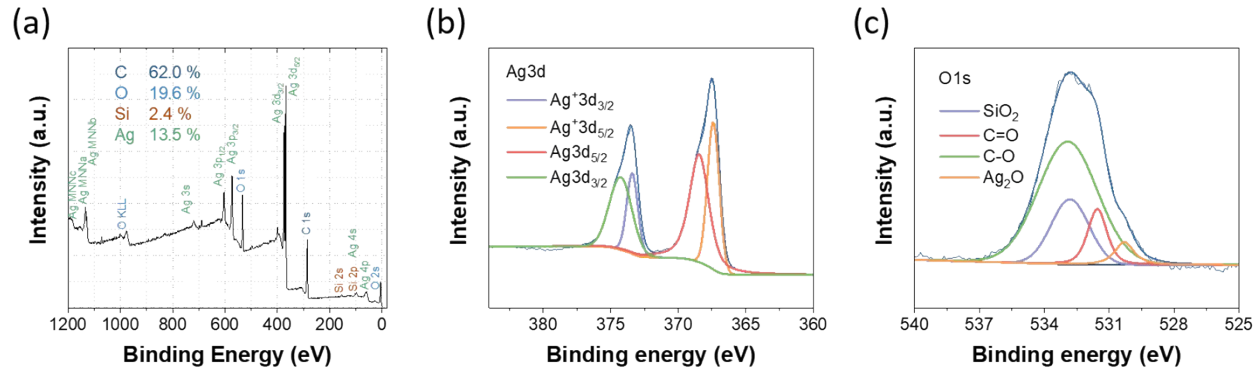

Figure S3. XPS spectra of the elements of AgNPs@SiO_2@cotton. (a) Survey spectra. High-resolution spectra of (b) Ag3d and (c) O1s. Note: the total element composition in (a) is not 100%, which may be induced by the impurities of b-PEI.

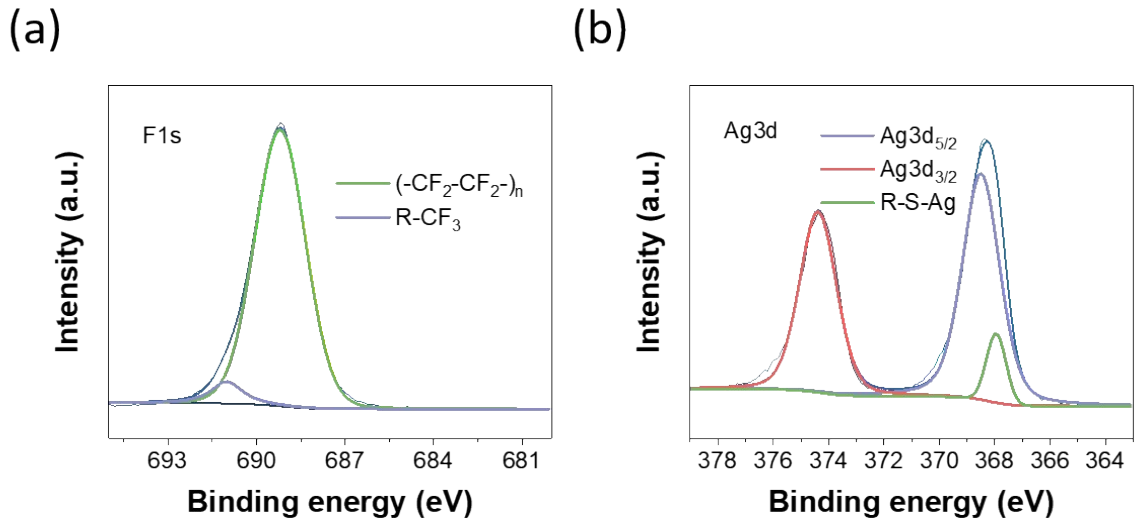

Figure S4. High-resolution XPS spectra of the elements of the omniphobic AgNPs@SiO_2@cotton encapsulation layer. (a) F1s spectra and (b) Ag3d spectra.

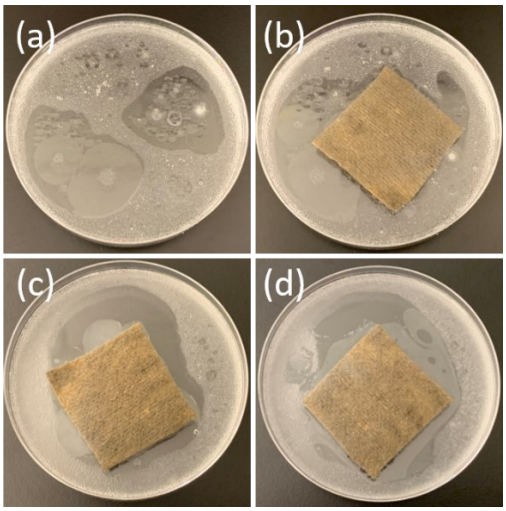

Figure S5. Digital photos of the wetting test in oil-water mixture. (a) Oil-water mixture. Fabric floating on the surface of oil-water mixture at t=0 h (b), 24 h (c), and 48 h (d).

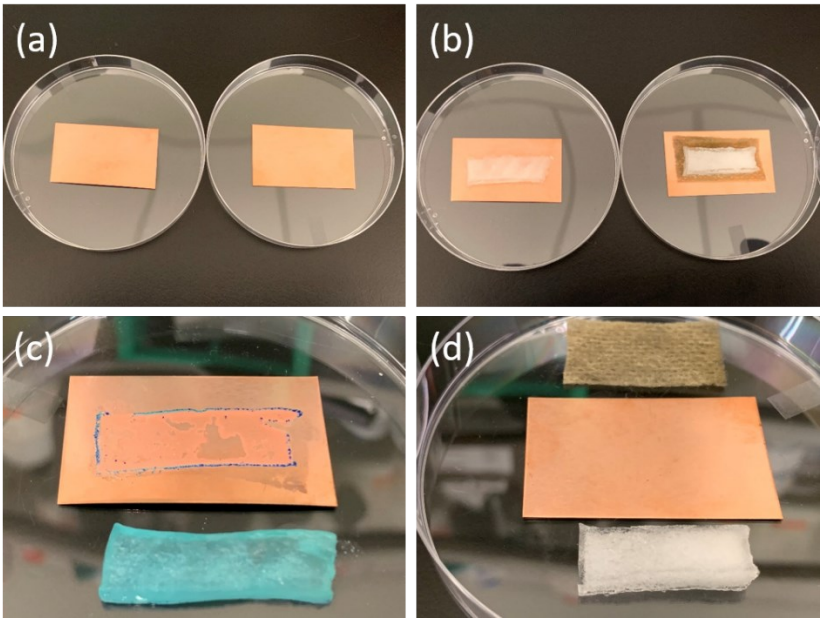

Figure S6. Digital photos of the corrosion evaluation test. (a) Copper plate prior to the test. (b) Left: PAM-$CaCl_2$ hydrogel and the copper plate were in direct contact; right: PAM-$CaCl_2$ hydrogel on top of the omniphobic AgNPs@SiO_2@cotton fabric, which was on direct contact of the copper plate. (c) Digital photo of the copper plate and PAM-$CaCl_2$ hydrogel in direct contact for 2 months. (d) Digital photo of the copper plate after being in contact with the setup in (b) for 2 months, with the omniphobic AgNPs@SiO_2@cotton fabric and PAM-$CaCl_2$ hydrogel being shown separately.

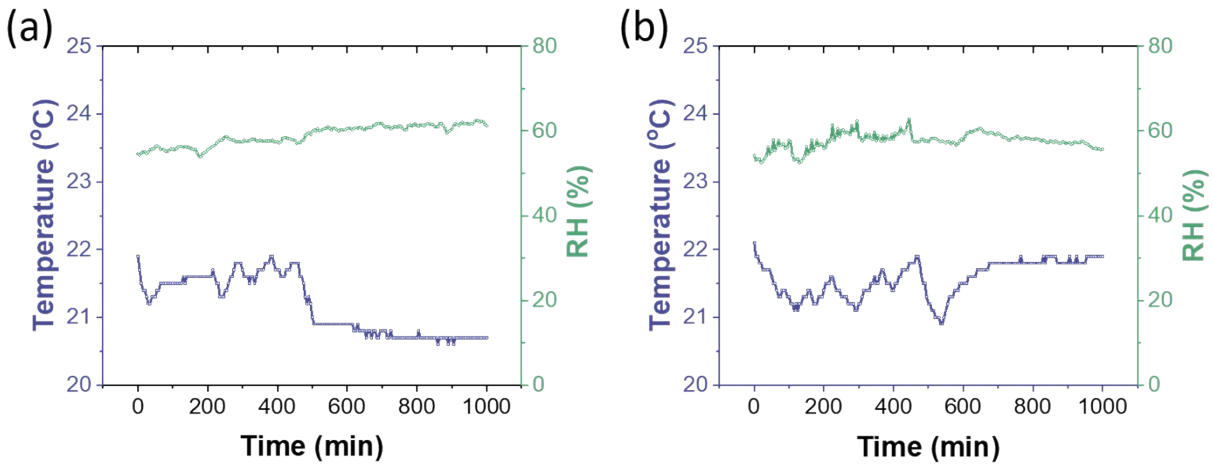

Figure S7. Actual environment conditions for the water vapor sorption test. (a) SWEAPS and (b) PAM-$CaCl_2$ hydrogel.

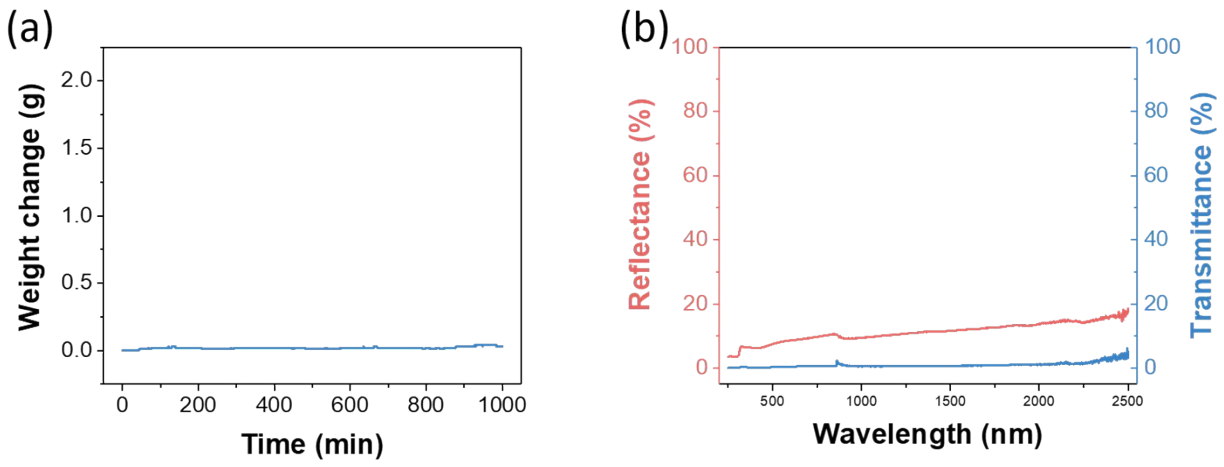

Figure S8. (a) Water vapor sorption property of the omniphobic AgNPs@SiO_2@cotton fabric. (b) UV-vis-NIR spectrum of omniphobic AgNPs@SiO_2@cotton fabric.

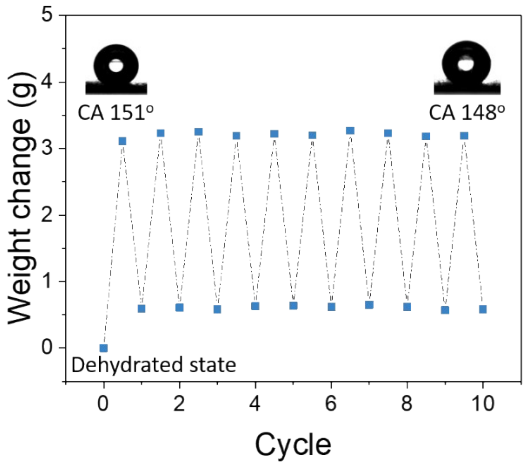

Figure S9. Cycling test results of water uptake and water release process. Insert are the CA image of the omniphobic encapsulation layer before (left, 151°) and after (right 148°) the cycling test.

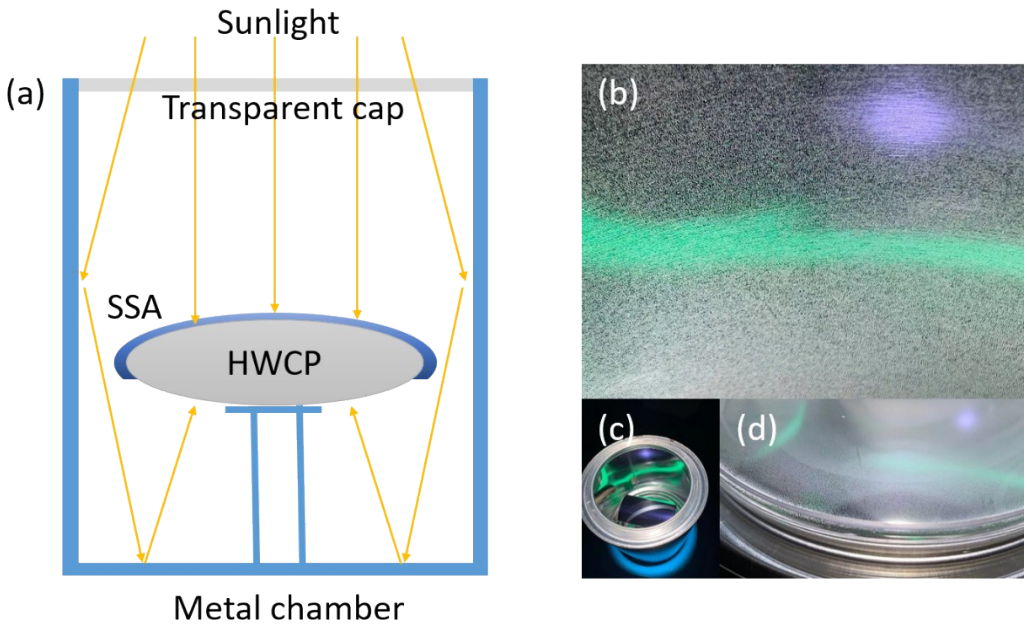

Figure S10. (a) Schematic of the device for water desorption and collection process. (b) Digital photo of the condensed water droplets inside the metal chamber. (c) Digital photo of photothermal chamber at the initial state. (d) Digital photo of the condensed water droplets inside the transparent cap.

Supplementary note 1. Characterization and Details of DVS test

Characterization

Scanning electron microscope (SEM) images and energy-dispersive X-ray spectroscopy (EDS) mappings were obtained on Teneo VS SEM (Thermo Fisher Scientific). The high-resolution transmission electron microscope (HRTEM) image was obtained on a Titan Themis Z TEM (FEI). X-ray photoelectron spectroscopy (XPS) analysis was carried out on a Kratos AXIS supra XPS spectrometer. Contact angle measurements were conducted on an OCA 35 (DataPhysics Instruments) contact angle meter at room temperature by using a 5 μL droplet as the indicator. The metal content in the produced water samples was measured on an inductively coupled plasma optical emission spectroscopy (ICP-OES, Agilent 5100) equipped with a charge-coupled and charge injection device. The total organic compound (TOC) and total nitrogen (TN) measurements were performed on a TOC-L (Shimadzu) analyzer. Infrared (IR) images were taken by a FLIR A655 IR camera. Dynamic water vapor sorption (DVS) test was conducted on a NETZSCH Jupiter simultaneous thermal analyzer (STA)-449 system, coupled with a modular humidity generator (MHG32, ProUmid).

Details of DVS test

The DVS test was conducted at 25 ^{o}C. The samples were pre-dried in an oven at 80 ^{o}C for 3 hours followed by quickly transferring it into the STA chamber. The sample was then in-situ dried at 80 ^{o}C for 2 hours at RH < 1% to further remove the residual water. The humidity was controlled by the humidified nitrogen gas that was purged into the STA chamber at a flow rate of 100 mL/h. The humidity range was set to be 10%-80% with 10% interval at each step, and the duration of the test at each humidity was set to be 4 hours.

Supplementary note 2. Theoretical models

Section 1. Humidity distribution above water surface.

In the first section of the theoretical model, COMSOL Multiphosics® simulation software was used to investigate the humidity distribution above the surface of bulk water. The structure of the modelled sectionis was shown in Figure S10a and b. The water surface with a dimension of 4 × 2.4 m^2 was placed in a wind field with defined humidity and wind speed. Both the temperatures of

water and wind flow were set to be 25 °C. The red plane in Figure S10a and b are the cut plane that were displayed in the simulation results. The airflow is modeled as turbulent flow and both the velocity and the pressure fields are assumed independent of air temperature and moisture.

The Moisture Transport in air (MT) interface was used to evaluate the amount of water evaporated from the water surface. The Evaporation Flux (EF, kg/m^2·s) can be described by equation (S1):

$$EF = K(c_{sat} - c_v)M_v \qquad \text{(S1)}$$

Where K is the evaporation rate constant (m/s), c_{sat} and c_v are the saturation concentration and the vapor concentration (mol/m^3), respectively. M_v is the molar mass of water vapor (kg/mol). The evaporation rate constant K, in the simulation was set to be large enough (i.e. 100 m/s) to ensure that the evaporation time scale is much smaller than that of diffusion/transportation time scale. At the water-air interface, the saturation concentration c_{sat} is assumed which can be calculated from equation (S2)

$$c_{sat} = \frac{P_{sat}}{RT} \qquad \text{(S2)}$$

Where P_{sat} is saturated pressure (Pa), R is gas constant, and T is temperature in Kelvin (K). The transport of water vapor is based on turbulence model in which the diffusivity can be expressed by equation (S3)

$$D_v = \frac{v_T}{Sc_T} I \qquad \text{(S3)}$$

Where D_v is diffusion coefficient (m^2/s), v_T is the turbulent kinematic viscosity (m^2/s), Sc_T is the turbulent Schmidt number, and I is the unit matrix.

In the simulation, the evaporation surface is set have the saturated vapor concentration. Theheat exchange across the water and air interface during the evaporation process is dominated by conduction, convection, and latent heat of water evaporation. Thereby, the Heat Transfer in Moist Air interface is applied in the simulation. To simplify the simulation, the initial temperature of the water and air flow are set to be constant at 293.15 K (20 °C). To investigate the influence of wind speed and wind humidity on the humidity distribution, two parameters were used to define the

wind field (wind speed, relative humidity): (1) 1 m/s, RH 40% and (2) 1 m/s, RH 80%. The humidity distribution across the water surface inside the wind field thus can be simulated.

As can be seen in Figure S10, the wind flow across the water surface significantly influences the humidity distribution. The high humidity region is significantly compressed and only occurrs within the region immediately close to and above the water surface. The humidity quickly declines to the value of ambient humidity away the high humidty region, implying the importance and need of floating SWEAPS directly on top of water surface to ensure high water update rate.

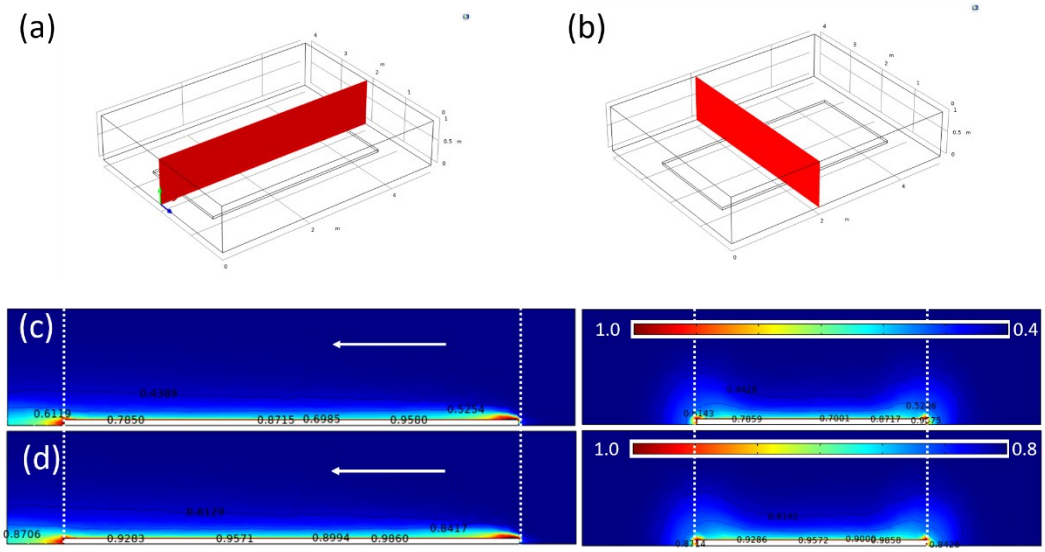

Figure S11. (a), (b) The dimension of the wind field and water surface. The red planes illustrated the cut planes that were displayed in the simulation results. (c), (d) Simulation results of the humidity distribution under (c) 1 m/s, RH 40%, and (d) 1 m/s, RH 80%. The white indicate the direction of the wind field. The height of each individual figure represents 1 meter in the simulation model.

Section 2. Driving force of water vapor transportation, sorption, and desorption.

The driving force of water vapor transportation, sorption, and desorption process is the vapor pressure difference between the water vapor sorbent inside the omniphobic fabric and the water source (denoted as "feed water") or the surrounding ambient. In this project, the active water vapor sorption component is hygroscopic salt $CaCl_2$. Since the polymeric parts do not contribute significantly to the water sorption performance, the composite hydrogel AWH sorbent is simplified

to be a $CaCl_2$ solution. The water vapor pressure difference (ΔP, Pa) can be expressed by equation S4.

$$\Delta P = \chi_{H_2O} \cdot P_s - P_{feed} \quad \text{(S4)}$$

Where the χ_{H_2O} is the molar fraction of water in $CaCl_2$ solution inside SWEAPS, P_s (Pa) is saturated water vapor pressure of $CaCl_2$ solution at the temperature of Ts (°C), P_{feed} (Pa) is the water vapor pressure at the feed side of SWEAPS. T (°C) is the feed media temperature. The calculation of P_{feed} can be further divided into two different conditions. When the feed is bulk water,

$$P_{feed} = (1 - \chi_{feed}) \cdot P_{s,\,feed} = \chi_{H_2O,feed} \cdot P_{s,\,feed} \quad \text{(S5)}$$

Alternatively, when the feed is ambient air,

$$P_{feed} = P_{s,\,feed} \times RH \quad \text{(S6)}$$

Where χ_{feed} is the molar fraction of non-volatile solutes in the feed media, $\chi_{H_2O,feed}$ is molar fraction of water in feed side. $P_{s,\,feed}$ (Pa) is the saturated vapor pressure at feed side, RH is the relative humidity of surrounding ambient. P_s and $P_{s,feed}$ can be calculated via Antoine's equation:

$$P_s = 133.32 \times 10^{\left(A - \frac{B}{C + T_s}\right)} \quad \text{(S7)}$$

$$P_{s,feed} = 133.32 \times 10^{\left(A - \frac{B}{C + T}\right)} \quad \text{(S8)}$$

Where A, B, and C are the constants, equal to 8.07, 1730.63, and 233.43, respectively. The constant 133.32 is the conversion of pressure unit from mmHg to Pa (1 mmHg = 133.32 Pa). The molar fraction of water χ_{H_2O} in $CaCl_2$ solution can be calculated by equations S9-S11

$$\chi_{H_2O} = \frac{n_{H_2O}}{n_{H_2O} + N_{ion} \cdot n_{CaCl_2}} \quad \text{(S9)}$$

$$n_{H_2O} = \frac{m \cdot (1 - F_{CaCl_2})}{M_{H_2O}} \quad \text{(S10)}$$

$$n_{CaCl_2} = \frac{m \cdot F_{CaCl_2}}{M_{CaCl_2}} \quad \text{(S11)}$$

Where n_{H_2O} and n_{CaCl_2} are moles of water and $CaCl_2$ in $CaCl_2$ solution, respectively. N_{ion} is 3 for $CaCl_2$, m is the total mass of the solution, F_{CaCl_2} is mass fraction of $CaCl_2$ in the solution, M_{H_2O} and M_{CaCl_2} is molar mass of water and $CaCl_2$, respectively. Similarly, the molar fraction, moles of water ($\chi_{H_2O,feed}$, $n_{H_2O,feed}$) and solutes (n_{feed}), and the mass fraction of solutes (F_{feed}) in feed water can be expressed by equations S12-S14.

$$\chi_{H_2O,feed} = \frac{n_{H_2O,feed}}{n_{H_2O,feed} + N_{ion,feed} \cdot n_{feed}} \quad \text{(S12)}$$

$$n_{H_2O,feed} = \frac{m \cdot (1 - F_{feed})}{M_{H_2O}} \quad \text{(S13)}$$

$$n_{feed} = \frac{m \cdot F_{feed}}{M_{CaCl_2}} \quad \text{(S14)}$$

Therefore, the water vapor pressure difference ΔP can be derived into equation S15 (feed side is bulk water) and S16 (feed side is ambient air).

$$\Delta P = \frac{n_{H_2O}}{n_{H_2O} + N_{ion} \cdot n_{CaCl_2}} \times 133.32 \times 10^{(A - \frac{B}{C + T_s})} - \frac{n_{H_2O,feed}}{n_{H_2O,feed} + N_{ion,feed} \cdot n_{feed}} \times 133$$

(S15)

$$\Delta P = \frac{n_{H_2O}}{n_{H_2O} + N_{ion} \cdot n_{CaCl_2}} \times 133.32 \times 10^{(A - \frac{B}{C + T_s})} - 133.32 \times 10^{(A - \frac{B}{C + T})} \times RH \quad \text{(S16)}$$

Since the concentration of $CaCl_2$ in the hydrogel is very high, a calibration function $f\left(F_{CaCl_2}\right)$ is established to correct the inaccuracy of colligative properties of the high-concentration solution. The calibration function is based on the comparison of the differences between the actual vapor pressure and calculated vapor pressure under different salt mass fractions and temperatures.

$$f\left(F_{CaCl_2}\right) = -1.56 \times F_{CaCl_2} + 0.42575 \times {F_{CaCl_2}}^2 + 1.1018 \quad \text{(S17)}$$

On the other hand, considering the fact that sodium chloride (NaCl) is the most abundant salt species in salted water, thus, NaCl solution is used as an example media in the following discussion of the theoretical model section to simulate the water with contaminants and impurities. When soluable impurities such as salt is added, the vapor pressure of the solution is lower than that of pure water. Thereby, water with different salt concentration will be discussed in this section. N_{ion} for NaCl is 2. Thereby, equation S16 and S17 are transformed into:

$$\Delta P = f\left(F_{CaCl_2}\right) \times \frac{n_{H_2O}}{n_{H_2O} + N_{ion} \cdot n_{CaCl_2}} \times 133.32 \times 10^{\left(A - \frac{B}{C + T_s}\right)} - \frac{n_{H_2O,NaCl}}{n_{H_2O,NaCl} + N_{ion,NaCl} \cdot$$

$$133.32 \times 10^{\left(A - \frac{B}{C + T}\right)} \quad \text{(S18)}$$

$$\Delta P = f\left(F_{CaCl_2}\right) \times \frac{n_{H_2O}}{n_{H_2O} + N_{ion} \cdot n_{CaCl_2}} \times 133.32 \times 10^{\left(A - \frac{B}{C + T_s}\right)} - 133.32 \times 10^{\left(A - \frac{B}{C + T}\right)} \times RH$$

(S19)

Equation S18 and S19 can be further derived into:

$$\Delta P = f\left(F_{CaCl_2}\right) \times \frac{\frac{(1 - F_{CaCl_2})}{18}}{\frac{(1 - F_{CaCl_2})}{18} + 3 \cdot \frac{F_{CaCl_2}}{111}} \times 133.32 \times 10^{\left(8.07 - \frac{1730.63}{233.43 + T_s}\right)} - \frac{\frac{(1 - F}{1}}{\frac{(1 - F_{NaCl})}{18}}$$

$$\times 133.32 \times 10^{\left(8.07 - \frac{1730.63}{233.43 + T}\right)} \quad \text{(S20)}$$

$$\Delta P = f\left(F_{CaCl_2}\right) \times \frac{\frac{(1 - F_{CaCl_2})}{18}}{\frac{(1 - F_{CaCl_2})}{18} + 3 \cdot \frac{F_{CaCl_2}}{111}} \times 133.32 \times 10^{\left(8.07 - \frac{1730.63}{233.43 + T_s}\right)} - 133.32 \times 1 \times RH$$

(S21)

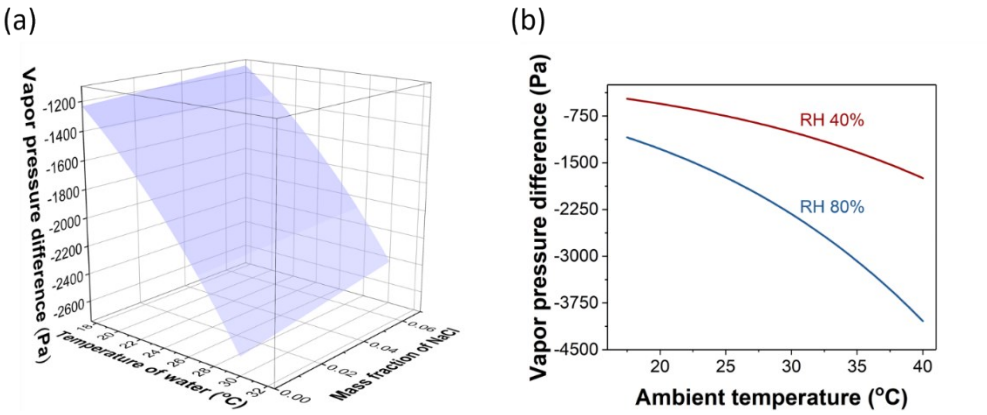

Figure S12. The calculated vapor pressure difference ΔP. (a) The feed side is liquid water; ΔP as a function of water temperature and mass fraction of non-volatile solutesin feed water (NaCl in this case). (b) The feed side is ambient air; ΔP as a function of ambient temperature under specific humidity.

ΔP < 0 indicates water vapor transfers from the feed side to the sorbent, and the more negative the value, the higher tendency of water vapor sorption. Figure S11a displays the calculated vapor pressure difference when the feed side is liquid water. The mass fraction of NaCl considered is between 0% and 7%, which covers the salinity of fresh water (0-0.05%), brackish water (0.05-3%), saline water (3-5%), and industrial brine water (> 5%). It is noteworhty that most of the salinity of brine water from RO plant is less than 7%. As can be seen, the vapor pressure difference highly depends on the temperature of water, while salt concentration contributes slightly to the value of ΔP within the range of the defined feed salinity. Figure S11b shows the relationship between ΔP and ambient temperature when the feed is ambient air under specific humidity conditions (i.e., 40 and 80% RH and wind speed of 1m/s). A distinct difference of ΔP can be found when the humidity is varied when the temperature is fixed. On the other hand, the absolute value of ΔP in the case of liquid water is higher than that of the humid air (of 80% RH), indicating the

advantage of harvesting the vapor within the high humidty region right above the feed water surface.

Section 3. Mass transfer

Mass transfer model is further build based on the discussions in the previous sections to reflect the water vapor transport, sorption and desorption dynamics across the boundary layer and omniphobic fabric. Based on our previous study, there are at least ~10 wt.% of residual water remains inside the composite hydrogel after photothermal process to desorb the harvested water, which is used to calculate the initial mass fraction of $CaCl_2$. To simplify the calculation, vapor phase thin film model (Figure S12a) is used. It is assumed that the feed media flows across a flat plate surface. Considering the dimension of the portable device in practical scale, along with the regular wind velocity of the outdoor environment, a laminar boundary layer is assumed in the modeling. Due to the large porous (i.e., ~50 μm based on SEM observation) and thin structure (i.e., ~ 0.17 mm in thickness measured by spiral micrometer) of the omniphobic fabric, we assume the transportation of water vapor across the fabric does not face significant resistance. The mass transfer process can be expressed by Fick's Law shown in equation S22.

$$J_v = -D_v \cdot \frac{d_c}{d_l} = \frac{D_v}{l} \cdot (c_i - c_{feed}) \qquad \text{(S22)}$$

Where J_v is the mole flux of water vapor (mol/(m^{2}s)), D_v is the diffusion coefficient of water vapor in air (m^2/s), l is the diffusion length (m), c_i and c_{feed} are the water vapor concentration in the hydrogel surface and in the feed side (mol/m^3). The moles of water vapor transferred (Nv) can be expressed by equation S23.

$$\frac{d_{N_v}}{d_t} = J_v \cdot A = \frac{D_v}{l} \cdot (c_i - c_{feed}) \cdot A \qquad \text{(S23)}$$

Where t is time, A is surface area of the hydrogel (m^2). Based on the ideal gas law, c_i and c_{feed} can be calculated as follows:

$$c_i = \frac{\chi_{H_2O} \cdot P_s}{R \cdot (T_s + 273.15)} \qquad \text{(S24)}$$

$$c_{feed} = \frac{P_{feed}}{R \cdot (T + 273.15)} \qquad \text{(S25)}$$

Where R is the gas constant (8.314 J/(mol·K)), χ_{H_2O} is the molar fraction of water in $CaCl_2$ solution in SWEAPS, P_s (Pa) is saturated water vapor pressure of $CaCl_2$ solution at the temperature of Ts (^oC), P_{feed} (Pa) is the water vapor pressure right above the feed water (i.e., outside the SWEAPS) with a temperature T (^oC).

The diffusion length l can be divided into two sections. One is the thickness of boundary layer on top of SWEAPS (l_1) and the other one is the thickness of the omniphobic encapsulation layer (l_2). l_1 can be calculated by equation S27

$$l = l_1 + l_2 \qquad \text{(S26)}$$

$$l_1 = \frac{\sqrt{A}}{0.646 \cdot (\frac{U\sqrt{A}}{v})^{1/2} \cdot (\frac{v}{D_v})^{1/3}} \qquad \text{(S27)}$$

Where U is the velocity of air (m/s), D_v is diffusion coefficient of water vapor in air (m^2/s), v is the viscosity of air (m^2/s), and A is the surface area of SWEAPS exposed to the feed water (m^2). Thus, equation S23 can be expressed by weight change as shown in equation S28.

$$\frac{d_m}{d_t} = \frac{D_v}{l_1 + l_2} \cdot (c_i - c_{feed}) \cdot A \cdot M_{H_2O} \qquad \text{(S28)}$$

Where m is the total mass of $CaCl_2$ solution, M_{H_2O} is the molar mass of water. Since the molar fraction of water varies throughout the sorption/desorption process, ideally, it should be measured experimentally with high accuracy. However, in this section, averaged molar fraction is used in the modeling for estimation.

$$\chi_{H_2O} = \frac{\chi_{H_2O,equilibrium} - \chi_{H_2O,initial}}{2} + \chi_{H_2O,initial} \qquad \text{(S29)}$$

$$F_{CaCl_2} = \frac{F_{CaCl_2,initial} - F_{CaCl_2,equilibrium}}{2} + F_{CaCl_2,equilibrium} \quad \text{(S30)}$$

Where the subscripts "initial" and "equilibrium" indicate the mole concentration of water and mass faction of $CaCl_2$ at the initial (the time when the water vapor sorption/desorption starts) and equilibrium state, respectively. When SWEAPS facing to ambient air, the mass transfer process can be expressed by equation S31.

$$\frac{d_m}{d_t} = \frac{D_v}{\frac{\sqrt{A_a}}{0.646 \cdot (\frac{U\sqrt{A_a}}{v})^{1/2} \cdot (\frac{v}{D_v})^{1/3}} + l_2} \times (\frac{\chi_{H_2O} \cdot P_s}{R \cdot (T_s + 273.15)} - \frac{RH \cdot P_{s,feed}}{R \cdot (T + 273.15)}) \times A_a \times M_{H_2O}$$

(S31)

Where A_a is the surface area of the device that is exposed to the ambient air. When SWEAPS facing to bulk feed water, the mass transfer process can be expressed by equation S32.

$$\frac{d_m}{d_t} = \frac{D_v}{l_2} \times (\frac{\chi_{H_2O} \cdot P_s}{R \cdot (T_s + 273.15)} - \frac{(1 - \chi_{feed}) \cdot P_{s,feed}}{R \cdot (T + 273.15)}) \times A_w \times M_{H_2O} \quad \text{(S32)}$$

Where A_w is the surface area of the device that is exposed to the bulk water. Due to heat conduction and convection, the surface temperature of the hydrogel is assumed to be equal to the temperature of the contacted feed media. Equation S31 and S32 can be further derived into equation S33 and S34:

$$\frac{d_m}{d_t} = \frac{D_v}{l_2} \times \left(\frac{\frac{\left(1-F_{CaCl_2}\right)}{18}}{\frac{\left(1-F_{CaCl_2}\right)}{18}+3\cdot\frac{F_{CaCl_2}}{111}} \cdot 10^{\left(8.07-\frac{1730.63}{233.43+T_s}\right)} \times f\left(F_{CaCl_2}\right) - \frac{\frac{\left(1-F_{NaCl}\right)}{18}}{\frac{\left(1-F_{NaCl}\right)}{18}+2} \right.$$
$$\left. \frac{}{R(T_s+273.15)} \right) \cdot 133.32 \cdot A_w \cdot 18$$

(S33)

$$\frac{d_m}{d_t} = \frac{D_v}{\frac{\sqrt{A_a}}{0.646\cdot\left(\frac{U\sqrt{A_a}}{v}\right)^{1/2}\cdot\left(\frac{v}{D_v}\right)^{1/3}}+l_2} \times \left(\frac{\frac{\left(1-F_{CaCl_2}\right)}{18}}{\frac{\left(1-F_{CaCl_2}\right)}{18}+3\cdot\frac{F_{CaCl_2}}{111}} \cdot 10^{\left(8.07-\frac{1730.63}{233.43+T_s}\right)} \times f\right.$$
$$\left. \frac{}{R(T_s+273.15)} \right.$$
$$\left. - \frac{RH\cdot 10^{\left(8.07-\frac{1730.63}{233.43+T}\right)}}{R\cdot(T+273.15)} \right) \cdot A_a \cdot 133.32 \cdot M_{H_2O}$$

(S34)

Supplementary Table S1 lists the essential parameters that are used for the calculation.

Supplementary Table S1. Parameters used for calculation of mass transfer process.

RH	F_{CaCl_2} equilibrium	F_{CaCl_2} initial	F_{CaCl_2}	F_{NaCl}	v m^2/s	U m/s	Aa m^2	Aw m^2	D_v m^2/s	R J/(mol·K)

40%	40%	85%	62.5 %	0-7%	1.5×10^{-5}	0-5	1.4	1	2.82×10^{-5}	8.314
80%	22%		53.5 %							
100% (water surface)	Close to 0%		42.5 %							

It should be noted that the assumptions and measurements are made to assist the calculation: (1) the dimension of the device is assumed $1 \times 1 \times 0.1$ m^3; (2) surface temperature of the hydrogel is equal to the contacted feed media; (3) l_2 is 0.17 mm based on the measuremnt.

The calculation results are presented in Figure S12b-d. The mass transfer rate, when the feed side is water, highly depends on the temperature of the feed water. Similar to the water vapor pressure difference, the mass fraction of non-volatile solute (i.e., 0-7%) in the feed at the defined salinity does not play an essential role (Figure S12b). When the feed side is ambient air (Figure S12c and d), the wind speed and the ambient temperature of the feed contribute similarly to the mass transfer rate. However, even when the humidity is doubled in Figure S13d, the overall mass transfer rate is still incompatible with the one with the feed being bulk water. A significant difference in mass transfer rate across the boundary layer can be observed between two types of feeds, indicating the importance of the floating SWEAP right above the feed water. The theoretical modelling framework developed in this work can be used to predict the water collection performance in pilot scale, assist designing large-scale devices, and optimize their configuration.

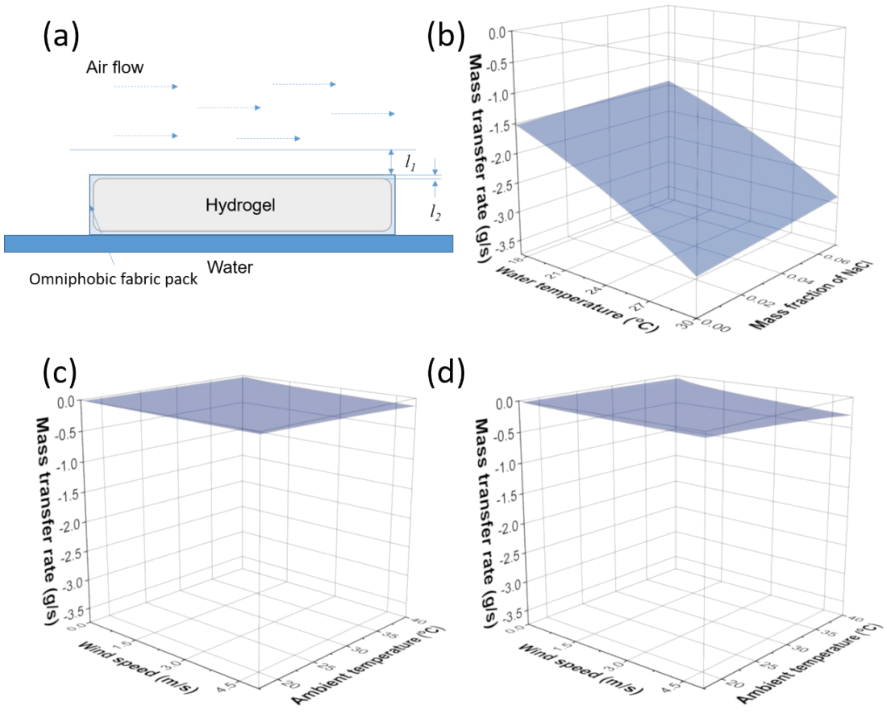

Figure S13. (a) Schematic of water vapor transfer to the hydrogel inside the SWEAPS. Calculation results of mass transfer process. (b) Mass transfer as a function of water temperature and mass fraction of non-volatile solute in feed side (NaCl in this case) when the feed side is water. (c), (d) Mass transfer as a function of wind speed and ambient temperature when the feed side is ambient air with relative humidity of 40% and 80%, respectively.

Supplementary note 3. Discussion on XPS analysis

The survey XPS spectra of cotton fabric show the carbon-to-oxygen elemental ratio is 2:1 (Figure S1a). The high-resolution XPS spectra of C1s of cotton fabric is shown in Figure S1b. Three components were fitted at the binding energy of 288.5, 286.5, and 284.4 eV, corresponding to C=C, C-O-C and C-C groups. The O1s (Figure S1c) components at 533.5 (C-O) and 532 (C=O) eV, further confirming the chemical composition. After being coated with SiO_2, silicon peak was observed at the survey spectra of SiO_2@cotton, and the decreased carbon-to-oxygen ratio could be attributed to the additional oxygen elements of SiO_2 (Figure S2a). A new peak was identified in the high-resolution XPS spectra of O1s at 533 eV, corresponding to SiO_2 (Figure S2b). Si2p spectra indicate that, despite SiO_2, SiO_x component also existed in the coating layer (Figure S2c). The survey spectra of AgNPs@SiO_2@cotton demonstrate the successful deposition of AgNPs; however, the total element composition in the spectra was not 100%, which can be attributed to the impurity presumably from b-PEI treatment (nitrogen peak could be observed at ~400 eV). Considering the fact that the averaged depth of XPS analysis is ~5 nm, the substrate element could be blocked by the coated b-PEI and AgNPs, which lead to the significantly changed carbon-to-oxygen ratio, along with the silicon ratio (Figure S3a). Four components were fitted in the high-resolution XPS spectra of Ag3d located at 374.3, 373.4, 368.5, and 367.4 eV, corresponding to $Ag3d_{3/2}$, $Ag^+3d_{3/2}$, $Ag3d_{5/2}$, , and $Ag^+3d_{5/2}$, respectively (Figure S3b). Ag_2O peak was fitted in the O1s spectra of AgNPs@SiO_2@cotton at 530.3 eV (Figure S3c) confirming the oxidation state of silver. After CVD deposition of perfluorosilane and perfluorodecane, a strong F1s peak, corresponding to 46.7% of surface chemical composition, was observed, indicating the successful deposition of the perfluoro-components. The sulfur peak in the spectra was corresponded to the thiol terminate of perfluorodecane (Figure 3a). The F1s spectra, fitted at the binding energy of 691 eV and 689 eV, confirmed the existence of $(-CF_2-CF_2-)_n$ chain and $R-CF_3$ group (Figure S4a). The newly identified peak at 368 eV in the Ag3d spectra corresponds to R-S-Ag, confirming the bounding of thiol-terminated perfluorodecane with AgNPs (Figure S4b).

Supplementary note 4. Cost estimation

Cost estimation was conducted based on the outdoor test results and the material prices at industry scale. The material cost for an individual SWEAPS that consists of 1.5 kg of PAM-$CaCl_2$ hydrogel and 1 m^2 of omniphobic fabric was estimated to be $12.32, which can produce at least 1 L of water from bulk water or 0.5 L of water from air during each daily cycle. Assumping SWEAPS has a lifetime of 1 years, and can produce at least 1000 L of water during its life span, the leverized cost of water is ~1.2 US cents per liter.

Table S2. Current price of industry-grade chemicals and materials for SWEAPS production

Name	Price (US dollars per kg)
TEOS	10
Cotton fabric	4
$AgNO_3$	350
Cit-Na	1.5
PVP	5
H_2O_2 30 wt%	0.41
$NaBH_4$	10
Methanol	0.22
2-propanol	1.3
Ammonium hydroxide	0.28
b-PEI	39
1H,1H,2H,2H-perfluorodecanethiol	200
1H,1H,2H,2H-perfluorooctyltriethoxysilane	1000
PAM	2
$CaCl_2$	0.3

Source:

https://www.1688.com/

https://www.alibaba.com/

Price estimation of SWEAPS based on 1 m^2 omniphobic fabric and 1.5 kg PAM-$CaCl_2$ hydrogel

Table S3. Material and chemical consumption and estimated price

Name	Consumption (g)	Price ($)
TEOS	150.4	1.504
Cotton fabric	120	0.480
$AgNO_3$	0.5	0.975
Cit-Na	13.9	0.021
PVP	0.139	0.001
H_2O_2 30 wt%	79.92	0.033
$NaBH_4$	0.738	0.007
Methanol (synthesis and wash)	3000	0.660
2-propanol	3537	4.364
Ammonium hydroxide	990	0.277
b-PEI	25	0.975
1H,1H,2H,2H-perfluorodecanethiol	2	0.4
1H,1H,2H,2H-perfluorooctyltriethoxysilane	1.663	1.663
PAM	0.3	0.6
$CaCl_2$	1.2	0.36
Total		**12.32**